International Journal of Rock Mechanics & Mining Sciences 69 (2014) 120–132

Contents lists available at ScienceDirect

International Journal of Rock Mechanics & Mining Sciences

journal homepage: www.elsevier.com/locate/ijrmms

Time-dependent deformation of shale gas reservoir rocks and its long-term effect on the in situ state of stress

Hiroki Sone [a,*], Mark D. Zoback [b]

[a] GFZ German Research Centre for Geosciences, Telegrafenberg, Potsdam 14473, Germany
[b] Department of Geophysics, Stanford University, Stanford, CA 94305, USA

ARTICLE INFO

Article history:
Received 12 July 2013
Received in revised form
3 March 2014
Accepted 7 April 2014

Keywords:
Gas Shale
Creep
Viscoelasticity
in situ stress

ABSTRACT

Laboratory testing of shale gas reservoir rocks reveal varying amounts of time-dependent viscous deformation in response to applied differential stress. The time-dependent deformation is an inherent property of the dry rock as it occurs in the absence of pore fluid. The contribution of the time-dependent deformation is generally larger for rocks with more clay and organic content. The time-dependent behavior can be modeled as a power-law function of time. Its magnitude is approximately linear with the magnitude of the applied differential stress and nearly insensitive to the confining pressure. By applying linear viscoelastic theory and using laboratory constrained constitutive parameters, we evaluated the effect of the time-dependent deformation in modifying the in situ differential stress over time. Modeling suggests that a significant proportion of a differential stress change would be relaxed over time-scales on the order of days. Because of this short time scale, the composition of the rock (as it influences the time-dependent behavior) may influence the in situ differential stress magnitudes stronger than the formation's geological loading history for these reservoirs.

1. Introduction

Characterization of the mechanical properties of reservoir rocks through laboratory testing often focuses on elastic properties for application to seismic and sonic data, or focuses on rock strength for application to problems such as wellbore stability. However, it is also important to understand the time-dependent inelastic properties of rocks in order to accurately predict the long-term behavior of reservoirs over time. Numerous laboratory studies have shown that deformation of weak reservoir sands and shales occur through elastic/viscoplastic constitutive behavior [1–5]. A significant portion of the deformation of these types of rocks takes place by a time-dependent response not predicted by linear elasticity. Failing to address the time-dependent response of these reservoir rocks may lead to significant errors in predicting reservoir compaction during depletion [6,7] and could lead to under-estimation of surface subsidence or inaccurate forecasting of reservoir performance.

In the study reported here, we investigated the time-dependent deformational properties of shale gas reservoir rocks. While shale gas reservoir rocks are relatively intact and exhibit much less time-dependent deformation than unconsolidated formations, it is still quite important for these rocks. For example, it has been suggested that hydraulic fractures in shale gas reservoirs may suffer from reservoir permeability loss due to time-dependent proppant-embedment [8,9]. As we show below, viscous deformation would be expected to appreciably affect the in situ state of stress as viscous flow relaxes differential stress. This not only affects the geomechanical response of the reservoir to processes such as hydraulic fracturing, but also may have important implications for the current state of stress that has developed over geological time. As shale gas reservoirs are known for their significant intra-reservoir heterogeneity [10], both lithological and mechanical, which may cause a variety of mechanical responses during hydraulic fracturing and production [11,12], it is important to properly assess the effect of time-dependent deformation and its controls to successfully understand/predict/optimize hydraulic fracturing operations for economical production.

We conducted laboratory triaxial creep experiments using natural shale gas reservoir rocks from several of the regions in North America where shale gas is being produced. In other studies, we report the static and dynamic elastic moduli, anisotropy, strengths, and general ductile behavior of the samples studied here [13,14]. The study reported here focuses on the time-dependent behavior and constitutive relations between stress, strain, and time. We then interpret the results in the framework of linear viscoelastic theory to quantitatively assess the geomechanical effect of viscous time-dependent deformation over engineering and geological time scales.

* Corresponding author. Tel.: +49 331 288 1324.
E-mail address: sone@gfz-potsdam.de (H. Sone).

http://dx.doi.org/10.1016/j.ijrmms.2014.04.002
1365-1609/

2. Methods

2.1. Sample description

We performed creep experiments using core samples from the Barnett, Haynesville, Eagle Ford, and Fort St. John shale. The material composition of these samples constrained by powder XRD analysis and pyrolysis is summarized in a ternary plot with clay+kerogen, QFP (quartz, feldspar, pyrite), and carbonate volumes as the end members (Fig. 1). Samples from Barnett, Haynesville, and Eagle Ford shale are further divided into 2 subgroups of distinct mineralogy where subgroup 1 contains more clay and organic contents than subgroup 2. In general, Barnett and Fort St. John shale samples are relatively QFP-rich and Eagle Ford samples are carbonate-rich. T_{max} obtained from Rock-Eval pyrolysis range in between 445 and 545 °C, indicating that organic matters in the shales are mature to over-mature (wet to dry gas). Sample porosity estimated from the average mineral density and the dry bulk density is between 1.5% and −9% and roughly correlates with the amount of clay and kerogen in the samples. There is significant anisotropy in the microstructure of these samples caused by the preferred orientation of clay minerals and the anisotropic shape/distribution of the solid organic matters which also introduces significant anisotropy in the elastic and deformational properties of these samples [13,14].

2.2. Laboratory procedures

We performed multi-step creep experiments in a servo-controlled triaxial apparatus to observe and examine the time-dependent mechanical properties of the samples. We used cylindrical samples of 1" diameter and 1.2–2.1" lengths, whose cylindrical axes were either perpendicular (vertical samples) or parallel (horizontal samples) to the bedding planes. Samples were first subject to a constant confining pressure of 10–60 MPa (above and below in situ effective pressure) and kept under the constant pressure for at least 3 h to reach thermal equilibrium inside the pressure vessel. Then differential stress, P_{diff}, of varying magnitude was applied in 2–5 steps by loading the sample in the axial direction. Each step of P_{diff} was applied over 60 s after which P_{diff} was held constant for 3 h to two weeks to observe the creep response of the sample. The differential stress applied by the differential load in the axial direction was kept below 50% of the ultimate rock strength to prevent the transition of the creep behavior into tertiary creep. Consequently, the creep deformation we observed only showed stable deformation with continuously decreasing strain rate. All samples were tested in "as received" conditions in order to best preserve the in situ hydration states. The mechanical responses we observed are expected to be free of any poroelastic effects as the fluid

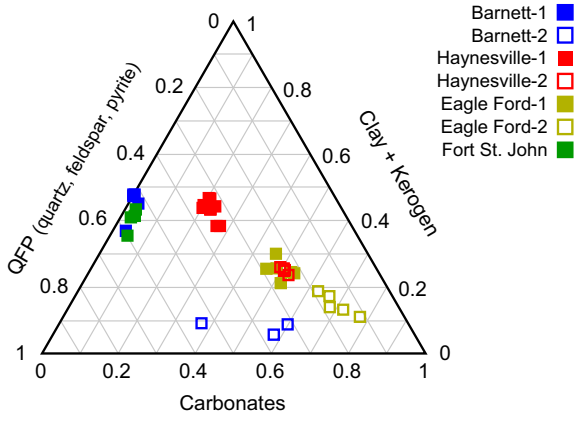

Fig. 1. Ternary plot representation of the sample material composition.

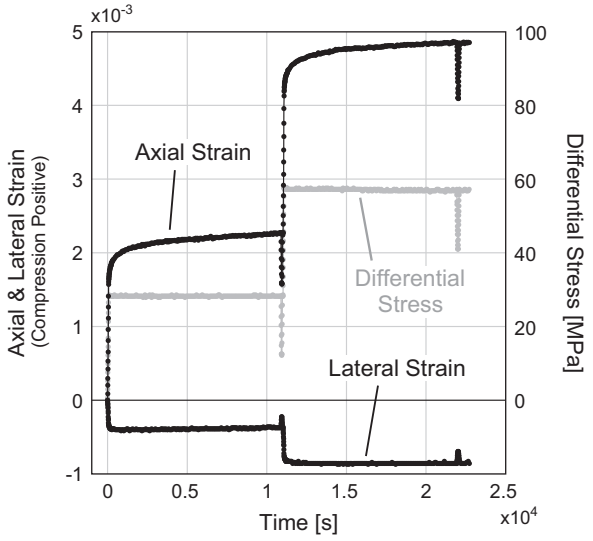

Fig. 2. Data from a representative experiment (Haynesville-1 vertical). In the axial strain data, the segment with sparse data points correspond to the strain data during application of the differential stress step.

saturation measured after recovery of the cores were at most 40% including clay bound water (discussed more in section 6.1). All experiments were conducted at room-temperature and drained pore pressure conditions.

During the experiments, sample deformation in the axial direction was measured by a pair of LVDT transducers and the deformation in the direction perpendicular to the axis (lateral deformation) was measured by a pair of spring-mounted strain-gauge transducers. Data from a representative experiment is shown in Fig. 2. In each step, most of the strain occurs in the initial 60 s while the axial differential stress is applied, mostly due to the elastic response of the rock, and the rest is the creep response under constant differential stress. A short term unloading and reloading of differential stress was inserted at the end of each creep deformation before moving on to the next pressure step, both done in 60 s, in order to measure the elastic modulus of the rock. From the slope of the stress-strain relation during the unloading and reloading, the Young's modulus was determined by least square linear regression.

As seen in Fig. 2, the lateral deformation exhibits much less time-dependent deformation during constant stress condition compared to the axial deformation. Thus majority of the time-dependent deformation takes place in the direction parallel to the applied differential stress. This was a common feature observed in all experiments. Since the scope of the paper is to investigate the first-order geomechanical impact of the sample time-dependent deformation, we will only focus on the axial deformation that takes place under triaxial stress condition.

3. Results

3.1. Observations of creep behavior

Several representative strain data upon a differential stress step are shown in Fig. 3. Axial strain is plotted relative to the strain value at the beginning of the differential stress step, thus includes both the instantaneous elastic and time-dependent creep response. A result from a test using a standard aluminum alloy sample is also shown as a reference for pure elastic behavior. We see that all samples exhibit some amount of time-dependent

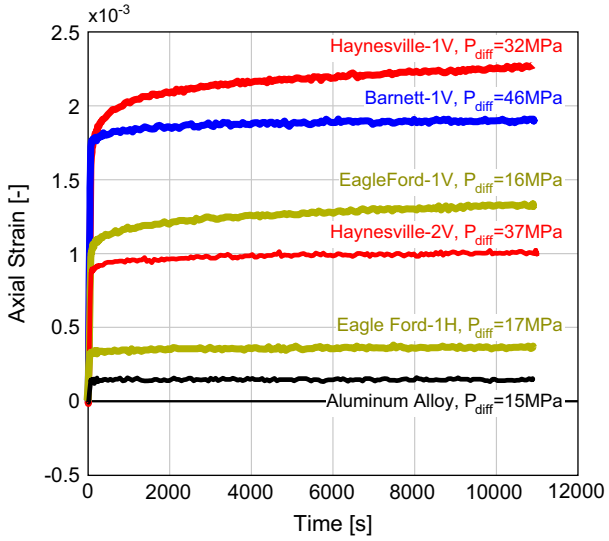

Fig. 3. Several representative 3 h creep data. P_{diff} indicates the amount of axial differential stress applied in the first 60 s. "V" denotes vertical samples, "H" denotes horizontal samples.

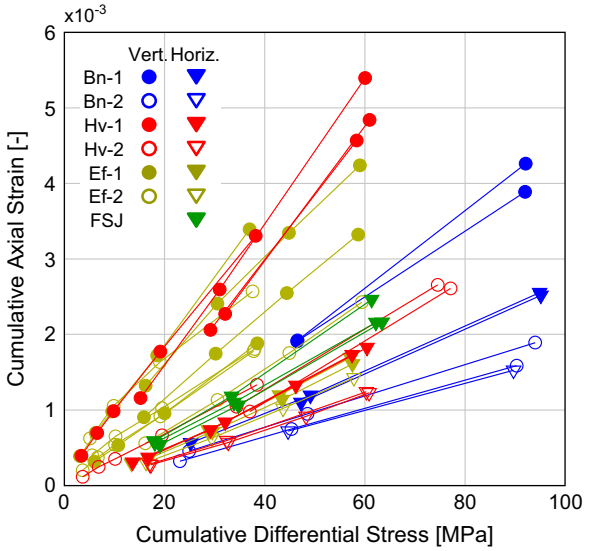

Fig. 4. Cumulative total axial strain vs. cumulative differential stress from 3 h hold data. Each connected plots represent an experiment from a single sample. Bn, Barnett; Hv, Haynesville; FSJ, Fort St John; Ef, Eagle Ford; Vert., vertical samples; Horiz., horizontal samples.

deformation and the creep strain continues to accumulate although at a continuously decreasing rate. Comparison of the data shows that there is significant variation in the strain responses. For instance, Hanesville-1 and Eagle Ford-1 vertical samples shows significant amounts of creep strain after 3 h, reaching up to about 30% of the initial immediate strain response observed in the first 60 s during the differential stress step, whereas other samples show much less creep strain relative to the initial strain observed in the first 60 s. We also see that when comparing samples from the same reservoir (e.g. Haynesville-1 vs. -2), the more clay- and organic-rich sample group tend to show much pronounced creep behavior. There is also anisotropy in the time-dependent behavior where vertical samples creep more than horizontal samples as illustrated by the two Eagle Ford samples in Fig. 3.

3.2. Pressure dependence of the strain response

Data from all experiments with 3 h hold times are plotted in Fig. 4, where the cumulative axial strain after each step is plotted against the cumulative axial differential stress. Each set of connected points represents data from an experiment using a single sample. We first note that the strain responses of these rocks are more or less proportional to the applied differential stress. This suggests that both the immediate elastic response and time-dependent creep response is roughly linear with differential stress at the relatively low stress levels tested. Note that Fig. 4 does not serve as a strict verification of linear behavior since we are neglecting the fact that creep strain from the previous steps continue in the subsequent steps. However, since majority of the creep deformation occurs within 3 h and much less in the subsequent hours, the trends observed in Fig. 4 indicate a first order linear differential stress dependence.

We also observe that the slopes indicated by samples of the same rock type and sample orientation are consistent with each other. This is despite of the different confining pressures, P_c, employed in each experiment. For instance, P_c varied between 10 and 60 MPa for the four Haynesville-1 vertical sample experiments (red filled circles), but the data points nearly overlap. This suggests that confining pressure is not a major control on the differential strain responses of these rocks. Fig. 5 further illustrates this point by comparing the 3 h strain responses from several Haynesville-1 samples where the strain data is normalized by P_{diff},

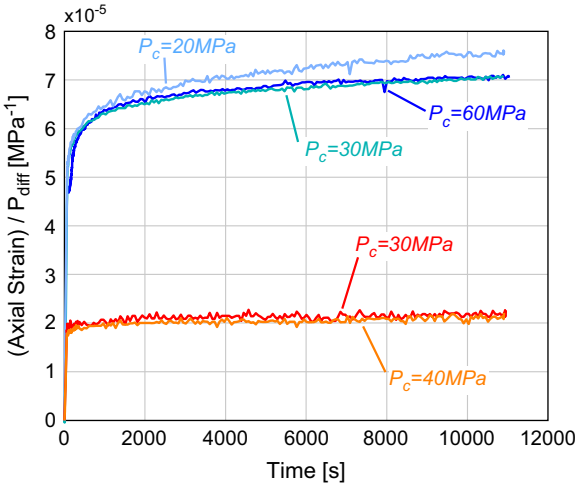

Fig. 5. Strain responses of Haynesville-1 vertical and horizontal samples. Data comes from the first differential stress step and is normalized by the magnitude of the applied stresses.

because the strain responses were found to be proportional to the applied differential stress from above. For both vertical and horizontal samples, the normalized strain responses nearly overlap with each other. Therefore the strain response of these shale gas reservoir rocks is linear against axial differential stress, P_{diff}, but not dependent on the confining pressure, P_c.

3.3. Hysteretic behavior during unloading/reloading stress steps

The linear dependence of strain against differential stress observed in Section 3.2 indicates the applicability of linear viscoelastic theory for the analysis of arbitrary time-dependent mechanical behavior of these samples. However linear viscoelastic behavior also implies that the creep behavior is reversible upon unloading of the applied stress change. In order to check if the shale samples obey this relation, we conducted one experiment with unloading/

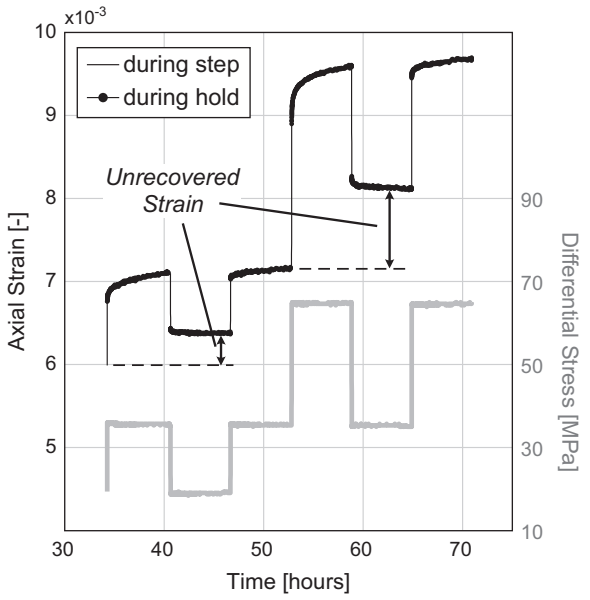

Fig. 6. Creep data from an experiment with unloading/reloading stress histories. A Haynesville-1 vertical sample was tested under 30 MPa confining pressure.

reloading differential stress paths using a Haynesville-1 vertical sample. In this experiment, the differential stress was held constant for an extended period of time between unloading and reloading of the differential stress, and also after reloading of stress (Fig. 6).

We observe from the strain data that there is significant hysteretic behavior. First, creep deformation appears to take place in the negative direction after unloading, but the magnitude and rate of creep strain upon unloading appears to be much smaller compared to the creep strain observed after the first-loading. There also appears to be a significant plastic component in the strain response during first-loading, indicated by the difference in strain level prior to the pressure step and the level where the strain appears to be approaching after unloading. Although a complete characterization of the hysteretic and plastic behavior requires further examination, these features suggest that the time-dependent deformation of the shale gas reservoir samples is most accurately described as being a combination of viscoelastic and viscoplastic behavior.

4. Characterization of viscoelastic behavior

In this section, we focus on the quantitative characterization of the time-dependent deformational behavior of the samples in the framework of linear viscoelastic theory. Although significant deviation from linear viscoelastic behavior is observed upon unloading (Section 3.3), linear behavior is observed during first-loading, such that there is no practical difference between viscoelasticity and viscoplasticity when only describing deformation during monotonic loading [4,6]. Therefore quantitative analysis through the application of linear viscoelastic theory can be instructive in assessing the geomechanical impact of the shale time-dependent deformation.

4.1. Linear viscoelasticity – Boltzmann superposition

Here we review some concepts in viscoelastic theory relevant to our analyses. For a complete review of the theory, see [15,16]. When a viscoelastic material is linear, the output strain (or stress) response scales linearly with the stress (or strain) input, and the principle of linear superposition holds (*Boltzmann Superposition*). Therefore, say the strain response to two instances of stress inputs is simply described as the sum of the two output strain responses resulting from each stress input. The linear superposition principle can be applied to obtain outputs from any arbitrary continuous inputs, by considering the continuous input as the sum of infinitesimal inputs. In that case, the output strain or stress responses can be described in an integral form as follows:

$$\varepsilon(t) = \int_0^t J(t-\tau)\frac{d\sigma(\tau)}{d\tau}d\tau, \quad \sigma(t) = \int_0^t E(t-\tau)\frac{d\varepsilon(\tau)}{d\tau}d\tau \tag{1}$$

where $J(t)$ is the creep compliance function which describes the time-dependent strain response to a Heaviside step input of unit stress, or a Dirac-delta input of unit stress rate. Similarly, $E(t)$ is the *relaxation modulus function* which describes the time-dependent stress response to a Heaviside input of unit strain, or a Dirac-delta input of unit strain rate. Eq. (1) describes that if the kernel responses, $J(t)$ and $E(t)$, are known, the responses to any arbitrary input history can be determined by convolving the kernel functions with the derivative of the input history. The analytical relationship between $J(t)$ and $E(t)$ can be seen by taking the Laplace transforms of Eq. (1), which yields

$$\varepsilon(s) = sJ(s)\sigma(s), \quad \sigma(s) = sE(s)\varepsilon(s) \tag{2}$$

By eliminating ε and σ from Eq. (2), we obtain the following relation between the creep compliance and the relaxation modulus in the Laplace domain:

$$E(s)J(s) = \frac{1}{s^2} \tag{3}$$

Eq. (3) is useful, as it allows us to obtain both $J(t)$ and $E(t)$ as long as one of them is constrained. However, Eq. (3) is only useful for solving $J(t)$ and $E(t)$ from one another when the Laplace and inverse-Laplace transform operations are manageable. Thus the most detailed and precise expression for $J(t)$ or $E(t)$ may not always be the ideal expression to carry out the viscoelastic analysis of interest. In the following sections, we focus on constraining the functional form of $J(t)$ and $E(t)$ that best describes our laboratory data and is practical for further analysis.

4.2. Obtaining the creep compliance function from laboratory data

We use the strain response observed from each differential stress step to infer the creep compliance function, $J(t)$. Although the raw strain data from each stress step is already a fairly close representation of the creep compliance function itself, the strain response we observe during and after the stress step does not strictly correspond to the kernel strain response because of the finite duration of the stress steps (60 s). The strain response right after the stress step will appear to lag from the true impulse response since the stress input was applied more slowly than a Heaviside function. In such case, it is customary in laboratory studies to discard the initial portion of the strain data and only analyze the remaining data to infer the creep compliance function, $J(t)$ [16]. Following this approach, we discard the initial 100 s of the strain data from each stress step. The remaining strain data was then divided by the magnitude of the stress step to obtain the creep behavior per unit input of differential stress. The outcome of this "cut and scale" procedure, which we refer to as the *creep compliance data*, now resembles the creep compliance function itself, the kernel strain response against unit input of stress step, thus has the units of MPa^{-1}. We found from an exhaustive comparison against a more exact approach, such as obtaining the creep compliance data based on Eq. (1) by deconvolving the strain data with the stress rate history [17], that the approximate approach we have utilized recovers the true creep compliance information very well.

4.3. Constitutive relation between time and strain

We are now interested in finding an analytical expression for $J(t)$. We note that our focus is not only to find an expression for $J(t)$ that simply fits the laboratory data, but also to find a model that has better long-term predictive capability. Given that most of our creep data only lasted for 3 h, it is important that a $J(t)$ function that we recover from the 3 h data can also reasonably predict the creep behavior for longer times.

Fig. 7 shows the creep compliance data in black from the longest experiment (2 weeks) conducted with a Haynesville-1 vertical sample, plotted against the logarithm of time ($\log t$ hereafter). Note again that the plotted data is simply the strain data without the first 100 s, normalized by the magnitude of the differential stress step. There are several key features of the sample creep behavior illustrated in Fig. 7. The data first shows that the creep compliance data continues to increase steadily with $\log t$ throughout the data. Thus creep strain continues and does not appear to reach any asymptote value even after 2 weeks. Also, there is no change in the smooth relation between creep compliance and $\log t$. Thus, there is no characteristic time scale for deformation and the time-dependence of the strain behavior is of a self-similar nature. This self-similar behavior also indicates the absence of the commonly observed "secondary creep" behavior [15,16] where creep strain rate reaches a stable rate after a characteristic duration time of the transient "primary creep" stage, perhaps because of the relatively modest differential stress levels applied.

These features suggest that common viscoelastic models composed of springs and dashpots, such as the Burgers or standard linear solid model are not suitable models to describe the observed creep behavior. Fig. 7 shows the regression of the Burgers and standard linear solid model (green and magenta curves) to the creep compliance data only up to 3 h. We do this to investigate whether a particular viscoelastic model can recover useful long-term information from just 3 h of creep data. As shown, both models can fit the data well up to 3 h but have poor ability to predict how creep continues beyond the 3 h regression time window. This is because creep behavior of all viscoelastic models composed of springs and dashpots either has a strain asymptote (long-term solid-like) or reach a stable strain rate (long-term liquid-like) after some characteristic time constant that describes the duration of the transient behavior. Therefore, these types of viscoelastic models cannot produce creep behavior that continues at a constantly decelerating rate over a wide range of time scales. One can combine multiple spring/dashpot elements possessing a range of different time constants for transient behavior in order to fit creep data at a wider range of time scale, but such an approach lacks uniqueness and overly complicates the viscoelastic model by adding indefinite number of spring/dashpot elements.

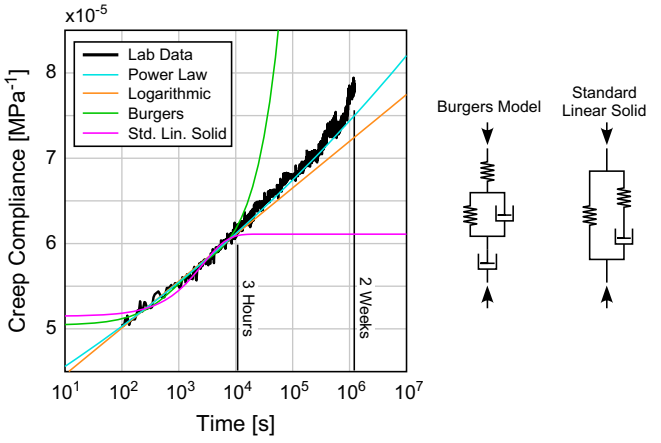

Fig. 7. Two-week long creep compliance data of a Haynesville-1 vertical sample and various constitutive relations. Power-law, logarithmic, Burgers model, and standard linear solid model constitutive models are fit to laboratory data up to 3 h.

As discussed above, there appears to be no characteristic time scales involved in the creep behavior and the experimental data shows a smooth monotonic trend throughout in the creep compliance versus $\log t$ plot (Fig. 7), implying a self-similar behavior in time. Some simple functions with self-similar characteristics are logarithmic and power-law functions which are commonly used to describe creep compliance of plastics and concrete materials [15]:

$$J(t) = A_1 + A_2 \log_{10}(t) \quad (A_1, A_2 : \text{constants}) \tag{4}$$

$$J(t) = Bt^n \quad (B, n : \text{constants}) \tag{5}$$

Since most of our creep compliance data lasted for 3 h where the data appears more or less linear (straight) in the plot, both functions appeared to be a good model to describe the data. However, we see from several weeks long creep data that a slight upward concavity starts to become evident after about 10^5 s which can only be captured by a power-law formulation (Fig. 7). For this reason, we find that the power-law can predict the long-term (2 weeks) behavior much better given only short-term (3 h) information as in most of our creep compliance data. Therefore, we choose the power-law formulation, Eq. (5), as the constitutive relation used to quantitatively characterize the time-dependent behavior.

4.4. Constitutive parameters from laboratory data

In order to recover the two constitutive parameters, B and n, in Eq. (5) from each laboratory data, each creep compliance data was fit by a straight line in the $\log t - \log J$ space (Fig. 8). This way, the slope and y-intercept recovered from the regression represents the value n and $\log B$, respectively. All results from the regression of Eq. (5) to each creep compliance data is plotted in Fig. 9 and its

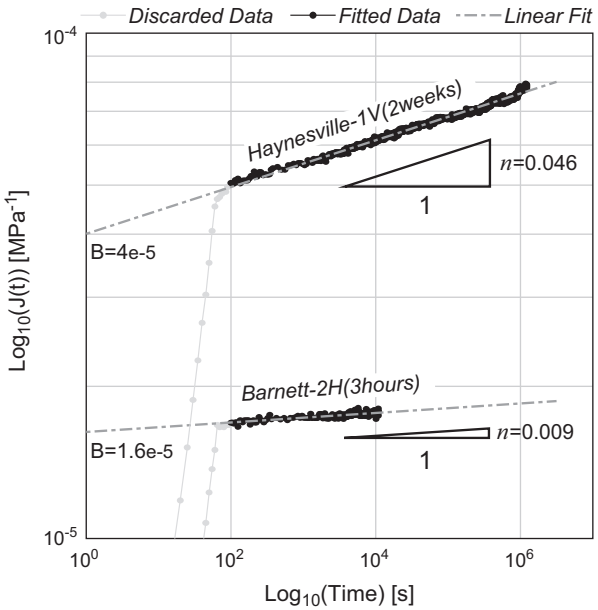

Fig. 8. Examples of linear regression performed in the $\log t - \log J$ space to determine the constitutive parameters, B and n. The grey data is the first 100 s which is not considered in the regression due to the proximity to the pressure step.

summary is provided in Table 1. Each panel shows the power-law exponent, n, plotted against B for each sample group. Since several pressure steps were conducted using a single sample, several pairs of B and n values are obtained for a single sample. The average of those values is shown by the circle and triangle plots, for vertical and horizontal samples, respectively. The range of B and n values

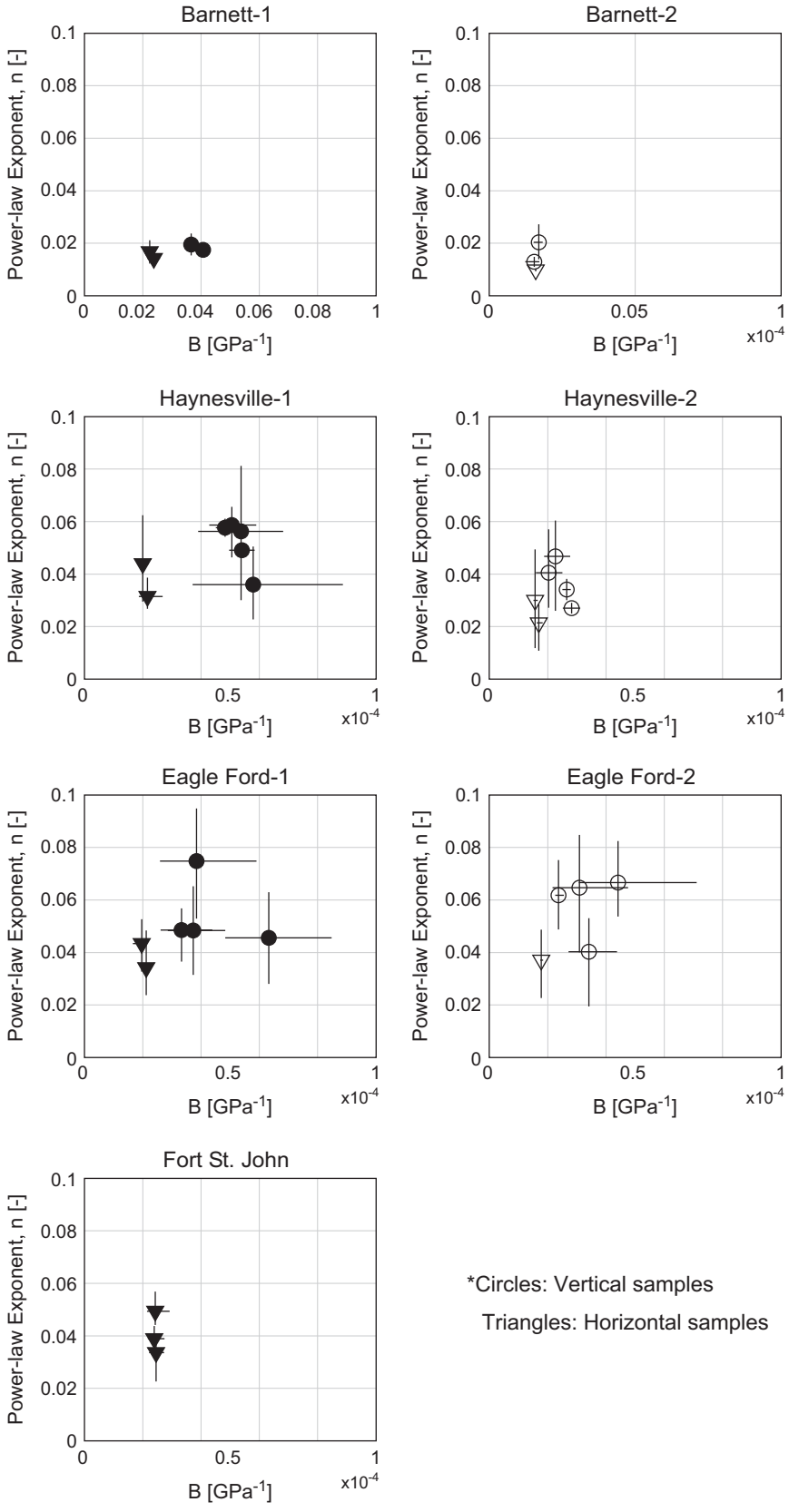

Fig. 9. Summary of the constitutive parameters determined from the creep compliance data. Each panel shows data from each sample group. Each data point represents the average value of the constitutive parameters determined for a single sample. The crosses represent the range of constitutive parameters observed in each sample.

Table 1
Power-law constitutive parameters recovered for each sample group.

Sample group	Vertical samples (bedding perpendicular)		Horizontal samples (bedding parallel)	
	B (10^{-5} MPa^{-1})	n	B (10^{-5} MPa^{-1})	n
Barnett-1	3.5–4.2	0.015–0.024	2.0–2.6	0.012–0.021
Barnett-2	1.2–1.8	0.011–0.027	1.6–1.6	0.009–0.010
Hayneville-1	3.7–8.9	0.023–0.081	1.8–2.7	0.027–0.062
Hayneville-2	1.6–3.1	0.025–0.060	1.5–1.8	0.011–0.049
Eagle Ford-1	2.6–8.5	0.028–0.095	1.7–2.3	0.024–0.053
Eagle Ford-2	2.2–7.1	0.019–0.085	1.7–1.8	0.023–0.049
Fort St. John	–	–	2.2–2.9	0.023–0.057

observed from a single sample is represented by the crosses, whose horizontal and vertical span represents the maximum and minimum values of B and n observed from a sample, respectively. Although some vertical samples from some sample groups (Haynesville-1, Eagle Ford-1, and Eagle Ford-2) tend to show wider variation of constitutive parameters recovered from a single sample, the constitutive parameters are fairly consistent for a given sample group and orientation.

Comparison between sample groups shows that different sample groups clearly possess different ranges of B and n values. For instance, Barnett shale samples possess relatively lower B and n values, whereas Haynesville and Eagle Ford samples show relatively higher B and n values. Within the same reservoir, it is generally seen that the relatively clay- and organic-rich sample group (subgroup 1) possess higher B and n values compared to the other. We also observe that vertical samples generally possess higher B and n values compared to the horizontal samples. Thus, there is anisotropy in the viscoelastic behavior just as there is elastic anisotropy in these samples [13].

4.5. Interpretation of the constitutive parameters

Although the power-law constitutive formulation shown in Eq. (5) was a heuristic choice for the creep compliance function, it is possible to give reasonable interpretations to the associated constitutive parameters, B and n. Eq. (5) indicates that constant B is the amount of strain that occurs after 1 s in response to a unit input of stress. Although Eq. (5) does not mathematically include a true instantaneous response, we find that B essentially reflects the instantaneous elastic property of the rock. Fig. 10 plots the inverse of B against the measured Young's modulus. Despite some scatter in the trend between the two quantities, an approximately 1-to-1 correlation is evident in the plots. Therefore, $1/B$ roughly correlates with the elastic Young's modulus, and thus B is a rough measure of the (uniaxial) elastic compliance of the rock. We call B the *compliance constant* having units of [MPa^{-1}]. The correlation between $1/B$ and Young's modulus probably results from the initial 1 s of creep deformation mostly reflects the instantaneous elastic deformation that occurs before any creep deformation takes place. It is possible to modify Eq. (5) to accurately reflect the instantaneous deformation at $t=0$. However, we keep the simple form in Eq. (5) because there are no practical differences in the long-term behavior between Eq. (5) and a formula that might be more accurate for the instantaneous deformation.

The power-law exponent, n, can be regarded as a parameter that describes the tendency to exhibit time-dependent deformation. If we regard the strain in the first 1 s as the elastic strain, n determines how much more time-dependent strain takes place.

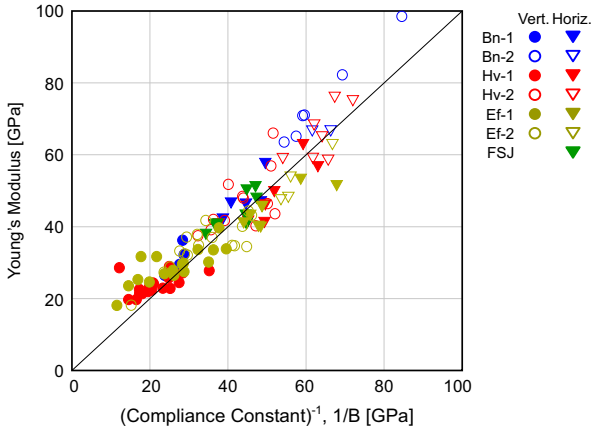

Fig. 10. Comparison between Young's modulus measured from stress-strain relation and stiffness of the rock inferred by the inverse of the compliance constant, B. Bn, Barnett; Hv, Haynesville; Ef, Eagle Ford; FSJ, Fort St. John.

For a unit input of stress $\sigma=1$ [MPa]:

$$\frac{\varepsilon(t)_{non-elastic}}{\varepsilon_{elastic}}=\frac{\varepsilon(t)-\varepsilon_{elastic}}{\varepsilon_{elastic}}=\frac{Bt^n-B}{B}=(t^n-1) \tag{6}$$

Therefore n determines the relative contribution of the time-dependent deformation to the total strain observed at a given time, t. Larger n values yield more pronounced creep behavior and $n=0$ yields no time-dependent deformation describing an elastic material.

4.6. Obtaining relaxation modulus from creep compliance

Given the power-law expression for the creep compliance function, we can obtain the relaxation modulus function, $E(t)$, under the assumption of linearity. Following the relations described in Eqs. (1)–(3), we perform a Laplace transform of the creep compliance function, solve for the relaxation modulus in the Laplace domain, then perform an inverse Laplace transform to obtain the relaxation modulus as a function of time:

$$J(t)=Bt^n$$
$$J(s)=\frac{B\Gamma(n+1)}{s^{1+n}}$$
$$E(s)=\frac{1}{s^2J(s)}=\frac{1}{B\Gamma(n+1)}\frac{1}{s^{1-n}}$$
$$E(t)=\frac{1}{B\Gamma(1+n)\Gamma(1-n)}t^{-n}\approx\frac{1}{B}t^{-n} \tag{7}$$

where $\Gamma(x)$ is the gamma function, and the final approximation is for $n\ll 1$. When $n=0.075$, the maximum value measured in the lab, the error introduced by the final approximation is 0.9%. We see from Eq. (7) that the relaxation modulus function also has a rather simple form such that $1/B$, corresponding to the Young modulus, determines the nearly instantaneous elastic stress response at $t=1$ s, and stress at later time is determined by multiplying a factor t^{-n} which decays over time. Thus n determines the fraction of the loaded elastic stress that remains un-relaxed after a given time. The constitutive parameters, B and n, in the relaxation modulus function are already constrained through the creep experiments. Thus we can discuss the stress relaxation behavior of the shale samples using values displayed in Fig. 9. Consistency of the constitutive parameters can be checked directly by conducting stress relaxation experiments, and it was found that values recovered from stress relaxation experiments are close to those recovered from our creep experiments [17]. This is an additional verification for linear viscoelastic behavior.

5. Geomechanical implications of long-term viscoelastic deformation

Through analysis of laboratory data, we have characterized the viscoelastic behavior of the shale gas reservoir rocks quantitatively by means of assigning power-law constitutive parameters, B and n, to each type of sample. We now use linear viscoelastic theory to evaluate its long-term effect on reservoir deformation and in situ stress.

5.1. Viscoelastic deformation at engineering time scales

We first discuss the effect of viscous deformation on geomechanical analyses at an engineering time scale. We do this by calculating the creep deformation and stress relaxation behavior, using the creep compliance and relaxation modulus functions, which would occur in one day, and also in one year, after sudden application of a stress and strain change. Such a time frame would be relevant, for instance, to the geomechanical calculation of stresses around wellbores used for wellbore stability analysis (days) or subsequent gas production (years) in shale gas reservoirs. We take the stress and strain steps as 10 MPa and 0.001, respectively, which are stress and strain magnitudes comparable to those introduced to a reservoir by drilling or fluid injection. These calculations allow us to assess whether analysis of reservoir deformation based on elasticity is accurate or not. However, because our analysis is one-dimensional, no geometrical boundary condition is considered, and also influence of pore pressure change is neglected, our results should be interpreted as a first order evaluation of the viscoelastic effect.

Results from one day viscoelastic deformation are shown in Fig. 11 overlaid on laboratory data of B and n constitutive parameters. In Fig. 11a, contours represent the amount of total strain that would occur in one day after a differential stress step of 10 MPa is applied to rocks with various combinations of B and n values. In Fig. 11a, where the contours intersect with the horizontal axis represents amount of strain due to purely elastic behavior since $n=0$ results in no time-dependent deformation. Contour values at the horizontal axis increase toward higher B values because B is proportional to the elastic compliance. Then as n increases in the vertical direction of Fig. 11a, contour values increase due to the increase in contribution from time-dependent creep deformation. Comparison of the laboratory data with the contours show that magnitudes of deformation (strain) after one day in most samples deviate significantly from the initial elastic deformation. From Eq. (6), (t^n-1) represents the additional strain that occurs relative to the initial elastic strain due to creep after a given time t [s]. For example, Haynesville-1 vertical samples with compliance constant values around 0.05 [GPa^{-1}] would initially respond elastically by a strain magnitude of 5e−4, but the strain doubles to about 1e-3 after one day due to additional contribution by creep (Fig. 11a, blue axis). Even for Barnett-2 samples with the lowest n values, thus least time-dependent behavior, 10% additional strain compared to the instantaneous elastic response occurs after one day.

In Fig. 11b, contours represent the amount of differential stress that would remain after one day from the application of a uniaxial

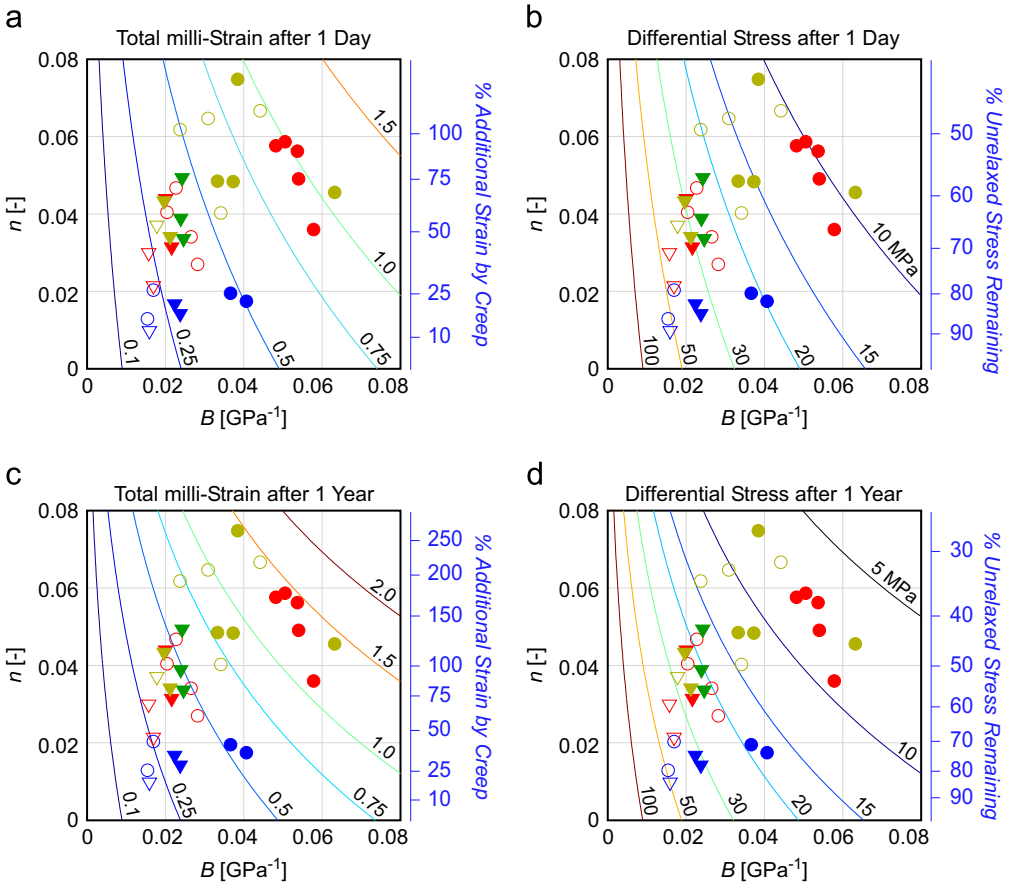

Fig. 11. Creep strain and stress relaxation response to a change of stress (10 MPa) and strain (1 milli-strain), respectively, over engineering time scale. Contours of stress and milli-strain are overlaid on laboratory data of B and n. (a) Total strain (elastic+creep) response after 1 day. (b) Differential stress after viscoelastic stress relaxation over 1 day. (c) Total strain (elastic+creep) response after 1 year. (d) Differential stress after viscoelastic stress relaxation over 1 year.

strain step of 1e−3. Again, where the contours intersect the horizontal axis represents purely elastic behavior. Because B is inversely proportional with the elastic modulus, contour values at the horizontal axis increase toward lower B values. Then contour values decrease towards higher n due to increasing stress relaxation behavior. Again, most samples deviate from elastic behavior already after one day. For Haynesville-1 samples, the elastic stress response is around 20 MPa but the stress relaxes to about 10 MPa just after one day. From Eq. (7), t^{-n} represents the fraction of the elastic stress that remains un-relaxed after a given time t [s]. Thus for instance, samples with $n > 0.04$ will relax at least a third of the initial elastic stress after one day (Fig. 11b, blue axis).

Results from 1 year viscoelastic deformation are shown in Fig. 11c and d. Contours showing amount of total strain and relaxed stress are similar to those in Fig. 11a and b, but show greater influence of the viscoelastic effect as expected from the longer time span considered. Contour values at the horizontal axis are identical to those in Fig. 11a and b since the elastic response is independent of time. However, the amount of creep strain or stress relaxation is greater compared to the results from one day viscoelastic deformation, so the contours are closer to horizontal in Fig. 11c and d.

We see from the results in Fig. 11 that the mechanical response of the studied shale gas reservoir rocks to changes of in situ stress and strain can be considerably different from pure linear elastic behavior. As the variation in n values indicate in Fig. 11, these rocks may behave different in the long-term although their immediate elastic behavior may be the same. Therefore, a geomechanical analysis of in situ stress and reservoir deformation may suffer from significant error if the time-dependent deformational properties of the reservoir rocks are not properly considered.

5.2. Stress accumulation over geological time scales

Now we attempt to apply the viscoelastic properties measured in the laboratory to study its effect on the current in situ differential stress. In the absence of structural complexity in the reservoir, current in situ differential stress, especially in the horizontal direction ($S_{Hmax} - S_{hmin}$), arises from the steady tectonic deformation at reservoir scale over geological time. Besides direct measurements of the minimum stress magnitude through mini-frac or leak-off tests, in situ reservoir stress magnitudes are oftentimes inferred from the elastic properties of the formation assuming simple gravitational loading, but results from Section 5.1 show that mechanical solutions based on elastic properties may not be applicable to processes that occur over time. Therefore, we honor the long-term process that leads to the accumulation of current stress states, and apply the superposition principle in Eq. (1) to infer the differential stress that would arise from a tectonic strain loading history. Such analysis makes a strong assumption on the validity of extrapolating laboratory data to geological time, and also leaves out some geological processes related to burial, diagenesis, maturation, and exhumation. Nonetheless, it can provide insight into the significance of viscoelastic deformation on the development of the current in situ state of stress.

5.2.1. Stress accumulation under constant strain rate loading

We start from the simplest tectonic loading history, a constant strain rate loading. In such case, the expression for strain in Eq. (1) simplifies to the following for a power-law relaxation modulus (Eq. (7)):

$$\sigma(t) = \int_0^t E(t-\tau)\frac{d\varepsilon(\tau)}{d\tau}d\tau = \int_0^t \frac{1}{B}T^{-n}\dot{\varepsilon}\,dT = \dot{\varepsilon}\frac{1}{B(1-n)}t^{1-n} \tag{8}$$

where $\dot{\varepsilon}$ represents the constant strain rate for tectonic loading. Thus given power-law constitutive parameters B and n from laboratory data, we only need to specify a value for the constant strain rate in order to know the differential stress accumulated at a given time t.

Here in our calculation we take t as 150 Ma which is approximately half of the age of Barnett shale. 150 Ma is approximately when diagenesis and maturation completed before uplift [18], and we believe this is a reasonable timing when the Barnett shale acquired its current mechanical properties. Different shale gas reservoirs clearly have different ages, but as it will become evident in Section 5.2.2, the exact duration of the tectonic loading defined by t is not so important as long as t does not vary by orders of magnitude between reservoirs.

We then constrain a reasonable tectonic strain by acknowledging that the shale gas reservoirs we studied are located within a stable intraplate region. The fact that plates are rigid over geological time provides an upper bound of intraplate strain rates of about $10^{-18}\,s^{-1}$ [19,20]. The lower bound can be estimated from the fact that about 30 MPa horizontal stress difference was observed from a vertical well in Barnett shale [17]. Since the horizontal Young's modulus of the Barnett shale reservoir rocks were found to be between 40–60 GPa, it requires that there has been at least $5–7.5 \times 10^{-4}$ elastic horizontal strain loaded over the age of the Barnett shale (300 Ma) in the absence of viscoelastic relaxation. These information yield a lower limit average strain rate of about $5–8 \times 10^{-20}\,s^{-1}$ strain rate. Considering these bounds on intraplate strain rates, we take the constant strain rate to be $10^{-19}\,s^{-1}$ in our analyses.

Differential stress accumulated over 150 Ma under $10^{-19}\,s^{-1}$ strain rate loading is shown as contours in Fig. 12 overlaid on laboratory data. The magnitude of the differential stress predicted for the studied samples reach up to 20 MPa, which seems to be consistent with those observed in Barnett shale [17]. Similar to Fig. 11, contour values along the horizontal axis correspond to elastic behavior and the effect of viscous deformation increases as n increases. We see that contours are closer to horizontal compared to the short-term calculations in Fig. 11 which indicates that the power-law exponent, n, has a greater influence on determining the current differential stress magnitude. When $n > 0.04$, the studied rocks sustain less than 5 MPa of differential stress regardless of the elastic modulus. Thus the in situ differential stress in some rock types may be regarded to be very small based only on their power-law exponent value without further consideration of

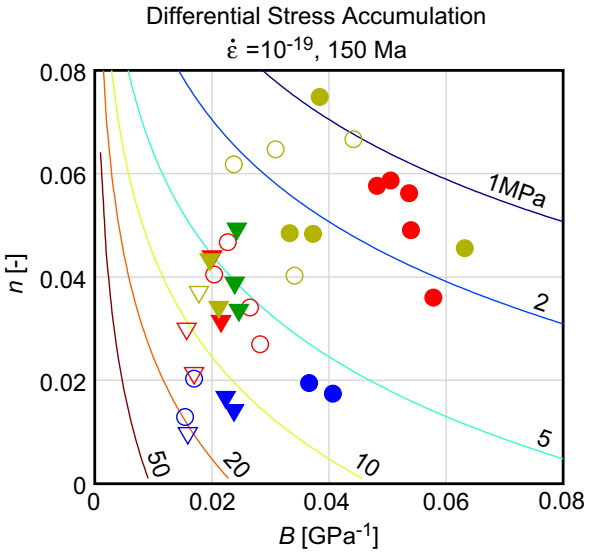

Fig. 12. Differential stress resulting from constant rate tectonic loading at 10^{-19} strain rate over 150 Ma. Contours representing differential stress magnitudes are overlaid on laboratory data of B and n.

its elastic properties. Because the variation in viscoelastic properties within a reservoir is controlled by the composition and fabric of the rock, lithology has a great influence on determining the in situ variation of differential stress.

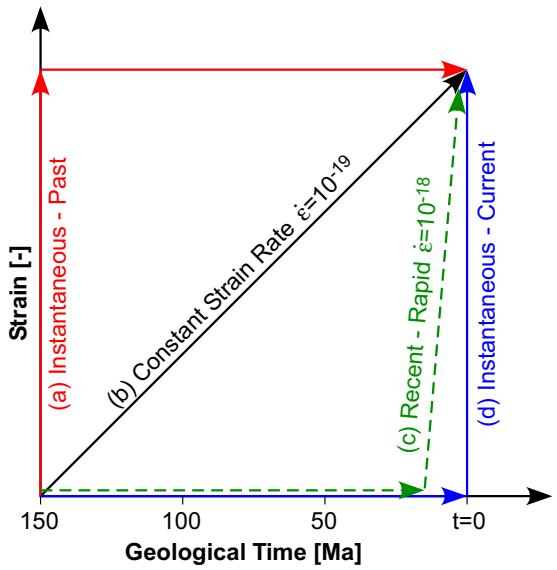

Fig. 13. Strain rate histories considered in the stress analyses for non-constant strain rate scenarios.

5.2.2. Influence of non-constant strain rate loading

Stress calculations from Section 5.2.1 were simplified by assuming a constant strain rate throughout time, but actual tectonic strain rates likely vary in time. Thus it is important to evaluate how results may deviate from the constant strain rate example under various scenarios of tectonic strain rate history. In order to cover the full spectrum of possibilities, we considered the differential stress accumulation caused by several extreme tectonic strain rate histories as shown in Fig. 13. In all cases, the total strain is the same as the example from Fig. 12, but the timing at which the tectonic strain occurs is varied. The "instantaneous-past" scenario represents all strain happening at the 150 Ma and then strain remaining constant throughout time. The "instantaneous-current" scenario represents all strain happening at the end of the history. The "rapid-recent" scenario represents all strain happening towards the end of the history at 10^{-18} s^{-1} strain rate.

Fig. 14 compares the results of the stress calculations from the instantaneous-past, constant strain rate (10^{-19} s^{-1}), recent rapid (10^{-18} s^{-1}), and instantaneous-current scenarios. Results show that there is very little difference in the calculated stress between the instantaneous-past, constant strain rate, and recent-rapid scenarios (Fig. 14a–c). Thus, any strain history path that lies in between the instantaneous-past and recent-rapid strain paths practically has no difference in the resulting current stress magnitudes. The instantaneous-current result is different from the others because it essentially shows the elastic response of the rock (Fig. 14d). There is no time for the stress to relax after the application of strain, and stress magnitudes are only dependent on the elastic modulus, hence

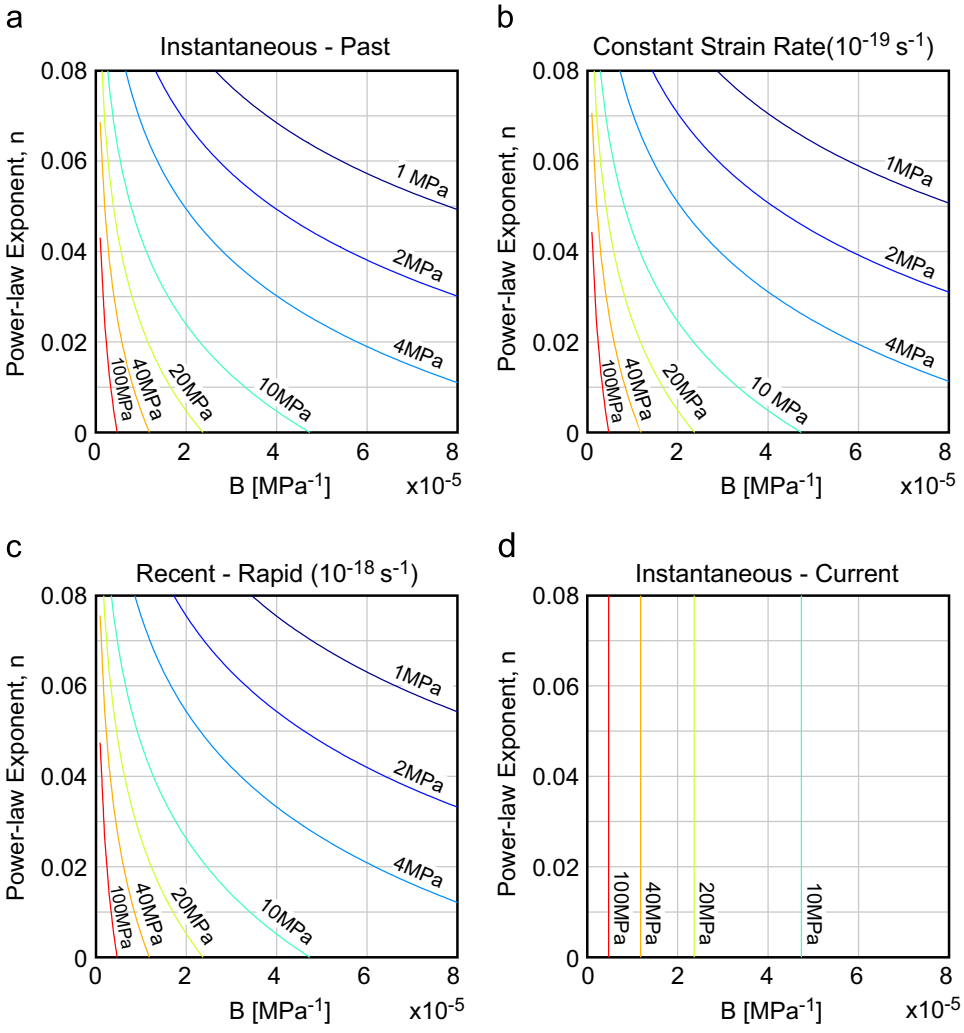

Fig. 14. Differential stress calculated for the four strain rate histories shown in Fig. 13. (a) instantaneous-past, (b) constant strain rate (10^{-19} s^{-1}), (c) recent-rapid (10^{-18} s^{-1}), and (d) instantaneous-current.

the vertical contours. However, unless we can obtain evidence that all tectonic loading occurred in the Quaternary period, it is unlikely that this is a realistic scenario.

These results suggest that the effect of variable strain rates is minimal for the purpose of analyzing the viscoelastic differential stress accumulation due to tectonic loading. This is because of the relatively short time scale required for the time-dependent behavior to become effective compared to long time scale of geological processes. Fig. 11 shows that significant viscous stress relaxation occurr after only one year. Therefore a stress calculation assuming a constant strain rate is sufficient enough to discuss the first order differential stress accumulation in these shale gas reservoirs.

6. Discussion

While the duration of laboratory creep experiments could approach time scales relevant to shale gas production (days to years), extending laboratory experiments to geological time scales (e.g. Section 5.2) requires an understanding of the physical mechanisms responsible for the creep. Rocks from shale gas reservoirs are extremely fine-grained and exhibit structures down to the nano-scale [21]. Furthermore, creep strains observed in our experiments are on the order of $1e-5$. Therefore, the deformational structures themselves are not easy to identify by simply comparing the pre- and post-experiment microstructures. In this section, we discuss some results that may provide useful insights in constraining the physical mechanisms involved in the time-dependent deformation of shale gas reservoir rocks.

6.1. The effects of water and the possibility of poroelastic effects

We conducted an additional experiment using a Haynesville-1 vertical sample dried in an oven at 100 °C for 3 months to study the effect of water on the time-dependent behavior. Change in sample weight after drying suggests that the water volume equivalent to about 1.5% of the total sample volume was dried off by this procedure. The sample porosity is estimated to be about 7%, so expelled water volume was about 20% of the pore volume. Based on the fluid saturation of approximately 20% measured from nearby samples, we suspect that essentially all of the free and clay-bound water present in the sample were dried by this heating procedure. The oven-dried sample was then deformed under an exactly identical stress history as another Haynesville-1 vertical sample that was kept under room-humidity condition. The results of the experiments are compared in Fig. 15.

We see that the relation between time and strain for the oven-dried sample can also be expressed by a power-law formulation (Fig. 15a). Also data from the oven-dried sample has a lower slope in the $\log t - \log J$ space and plots lower than the room-dry sample suggesting that less creep deformation takes place after removal of water. When the power-law constitutive parameters from these experiments are compared (Fig. 15b), we see that the main difference is in the power-law exponent, n, where the room-dry sample exhibit higher n values. On the other hand, the compliance constant, B, is about the same for the two samples. The room-dry sample may appear to have slightly lower B values on average, but given the variability of the B values measured from all Haynesville-1 vertical samples (Fig. 9), the difference between the oven-dried and room-dry samples is unresolvable. Since B reflects the elastic property of the rock and n reflects the time-dependent behavior of the rock, we can assume that the removal of water does not affect the elastic property of the rock, but affected the rate at which the creep deformation occurs.

Time-dependent deformations of rocks are sometimes attributed to poroelastic effects, when pore pressure changes induced by the whole rock deformation require time to equilibrate, especially if permeability is low or the viscosity of the pore fluid is high. The gradual equilibration of the pore pressure causes the rock to deform over time in response to the continuously changing pore pressure. Such effects are especially relevant for shales due to their low permeability [22].

However, we conclude that poroelastic effects did not play a significant role in the observed time-dependent behavior of the samples we studied. Not only was the water saturation of the samples quite low, the elastic response of the samples did not change, creep deformation was faster in room-dry samples and the total sample deformation is greater in the room-dry sample (Fig. 15a). If the presence of fluids in the room-dry samples caused any pore pressure disequilibrium, the effect should appear as a delayed and suppressed strain response compared to the oven-dried samples since enhanced pore pressure acts to resist sample volume loss. We consistently observed that the strain response of the room-dry samples preceded those from oven-dried samples after all pressure steps. This suggests that the dry frame of the rock inherently exhibits some time-dependent deformational behavior which is enhanced by the presence of water. Therefore our presumption that the fluid saturation is low enough to suppress poroelastic effects (Section 2.2) appears to be valid.

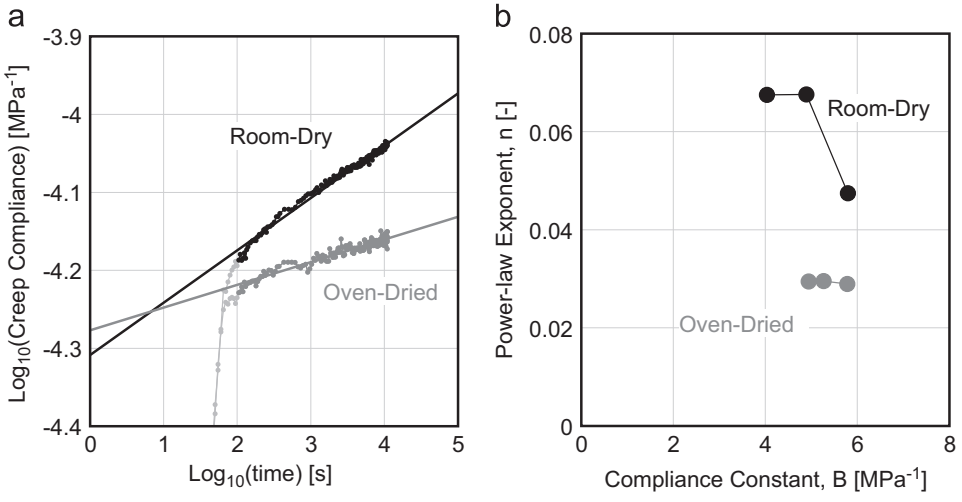

Fig. 15. Comparison of creep behavior of a room-dried and an oven-dried Haynesville-1 vertical sample. The oven-dried sample was dried at 100 °C for three months. (a) Comparison of creep compliance data from the third differential stress step. (b) Comparison of power-law constitutive parameters.

6.2. Insights into the physical mechanism of creep

As seen in Fig. 2, the time-dependent deformation occurs mainly in the axial direction and accommodated by a slight compaction of the samples. Inelastic compaction occurs as a result of grain rearrangement facilitated by the relative motion of the grains. The fact that the time-dependent creep behavior was affected by the amount of water in the pore spaces suggests that the physical mechanism responsible for the grain motion is a hydrolytically assisted mechanism. One possibility is that water is affecting the friction between the grains. Presence of water is known to lower the frictional coefficient of some minerals, especially clay minerals [23]. Thus grain motion by frictional sliding may have been more frequent in the room-dry samples resulting in enhanced creep deformation. However, the creep rate of the shales we studied was found to be independent of the confining pressure (Fig. 5), contradictory to the general characteristic of friction that shear strength is proportional to the normal traction. If frictional sliding was responsible for the creep deformation, we would expect that changes in confining pressure would influence the shear resistance between grain contacts and result in a change in creep rate. Therefore grain frictional sliding may not be a plausible mechanism.

Sub-critical crack growth is another deformation mechanism enhanced by the presence of moisture, which allows cracks to grow at sub-critical stress intensity factor levels with, for example, the assist of stress corrosion at crack-tips of silicates [24,25]. It is well-known that sub-critical crack growth produces time-dependent deformations of silica-rich rocks, for instance, “brittle creep” in granites and sandstones [26–28]. However, several aspects of our experiments do not match the expected behavior for sub-critical crack growth. First, the stresses applied in our experiments are much lower. In brittle creep experiments, the differential stresses applied to the samples are usually above 80% of the short-term rock strength. In our experiments, the applied differential stress applied was at most 50%, and mostly below 25%, of the short-term rock strength. Also the dependence of creep rate on differential stress is much higher than the linear dependence we found in our study. Results from Darley Dale sandstones [27], a clay-poor sandstone with about 13% porosity, shows increase in strain rate by an order of magnitude upon 10% increase of the applied differential load. Also sub-critical crack-growth has mostly been observed in quartz minerals in past studies, but the time-dependent deformation in our samples does not appear to correlate with quartz content. Our results show that the most quartz-rich samples from Barnett shale showed the least amount of time-dependent behavior (Figs. 11 and 12), and comparison between samples from the same reservoirs suggest that it is the amount of clay and/or organics that enhances the creep behavior. However, as microstructural observations have proven to be difficult so far for the identification of the deformation structure, we cannot identify for certain what mechanism was responsible for the observed time-dependent behavior. in situ observation of microstructures during experiments may be necessary to identify which mineral is deforming during creep in shale gas reservoir rocks.

6.3. Deviation from in situ conditions

Although our experiments were designed to deform the samples at stress states close to in situ conditions, several conditions in our experiments did not reflect reservoir conditions. For instance, the temperature at which the samples were tested was lower than in situ temperatures which can be higher than 100 °C in some shale gas reservoirs. Since ductile flow of minerals is usually understood as thermally activated processes (albeit at temperatures much higher than those relevant to shale gas reservoirs), the significance of time-dependent deformation could be larger at in situ temperatures than those represented in our experiments.

We also note that the time-dependent deformation we observed may have been enhanced slightly by the triaxial boundary condition (constant confining pressure acting on the side surface) in our experiments. Rocks in the subsurface are only subject to a constant stress boundary condition in the vertical direction because of the free ground surface but are subject to strain boundary conditions in the two horizontal directions. Although we observed that majority of the time-dependent deformation occurs in the direction parallel to the applied differential stress (Fig. 2), slight creep in the lateral direction was observed. If this creep in the lateral direction was suppressed by counter-forces associated with lateral strain boundary conditions, the samples may have exhibited smaller amounts of creep behavior. Application of experimental results to in situ geomechanical problems should improve from the development of a three dimensional tensorial description of the creep behavior.

7. Conclusions

We performed laboratory creep experiments using rocks from several shale gas reservoirs to investigate its time-dependent deformational behavior. We found that all samples exhibit time-dependent deformation of varying degree. The strain response was approximately proportional to the applied axial differential load, but was not dependent on the confining pressure, and the constitutive relation between strain and time is best described by a power-law function of time, $\varepsilon = \sigma B t^n$, with the power-law exponent varying between 0.01 and 0.09. Samples with higher clay and organic content exhibit more creep, thus higher n values, for a given shale gas reservoir. The majority of the time-dependent strain occurs in the direction parallel to the applied differential load, resulting in slight volume reduction during creep deformation. Because the presence of moisture was found to enhance creep deformation, the physical mechanism responsible for the time-dependent behavior appears to be a hydrolytically assisted compaction mechanism. The time-dependent behavior exhibits hysteretic behavior when samples undergo unloading/reloading stresses, and strain recovery upon unloading of stress appears to be slower compared to the creep strain rate upon loading.

A complete constitutive description of the observed viscoplastic behavior requires further laboratory testing under various loading conditions. However by only focusing on its effect during monotonic loading, we can still interpret our data quantitatively in the framework of linear viscoelastic theory. When the viscoelastic behavior is described by power-law creep compliance and relaxation modulus functions using laboratory-constrained constitutive parameters, we find that the mechanical responses of these rocks to a stress or strain change deviate significantly from linear elastic behavior even after one day. For the range of n values between 0.01 and 0.08, about 10–60% of the elastic differential stress change is relaxed after one day, and about 15–75% is relaxed after one year. Also for the same range of n values, about 10–150% additional strain occurs by creep after one day, and about 20–250% additional strain after one year. Calculation of current differential stress accumulated over geological time assuming constant strain rate tectonic loading recovers reasonable magnitudes consistent with field observations, and also shows the enhanced effect of the power-law exponent, n, in determining the current stress magnitude. Because calculations of the geological accumulation of differential stress is not influenced by the details of the tectonic loading history due to the relatively short time scale of stress relaxation compared to geological processes, the composition of the rock influencing the time-dependent behavior may have

greater control on in situ differential stress magnitudes than the formation's geological loading history.

Acknowledgments

We thank Paul Hagin and Norm Sleep for useful discussions, and ConocoPhillips, BP, and Unconventional Gas Resources for providing the samples used in this study. We also thank the reviewer for the constructive comments which helped to improve the manuscript. Financial support for Hiroki Sone was provided by the Stanford Rock and Borehole Geophysics (SRB) industrial consortium, Chevron, and ConocoPhillips.

References

[1] de Waal JA, Smits RMM. Prediction of reservoir compaction and surface Subsidence: Field application of a new model. SPE Formation Eval 1988:14214.
[2] Dudley JW, Myers MT, Shew RD, Arasteh MM. Measuring compaction and compressibilities in unconsolidated reservoir materials by time-scaling creep. SPE Reserv Eval Eng 1998:51324.
[3] Chang C, Moos D, Zoback MD. Anelasticity and dispersion in dry unconsolidated sand. Int J Rock Mech Min Sci 1997:34 (Paper No. 048).
[4] Hagin PN, Zoback MD. Viscous deformation of unconsolidated sands – part 1: time-dependent deformation, frequency dispersion, and attenuation. Geophysics 2004;69:731–41.
[5] Chang C, Zoback MD. Viscous creep in room-dried unconsolidated Gulf of Mexico shale (I): experimental results. J Pet Sci Eng 2009;69:239–46.
[6] Hagin PN, Zoback MD. Viscous deformation of unconsolidated sands – part 2: linear viscoelastic models. Geophysics 2004;69:742–51.
[7] Hagin PN, Zoback MD. Predicting and monitoring long-term compaction in unconsolidated reservoir sands using a dual power law model. Geophysics 2007;72:E165–73.
[8] Morales RH, Suarez-Rivera R, Edelman E. Experimental evaluation of hydraulic fracture impairment in shale reservoirs. ARMA Paper 2011-380.
[9] Alramahi B, Sundberg MI. Proppant embedment and conductivity of hydraulic fractures is shales. ARMA Paper 2012-291.
[10] Passey QR, Bohacs KM, Esch WL, Klimentidis R, Sinha S. From oil-prone source rocks to gas-producing shale reservoir – geologic and petrophysical characterization of unconventional shale-gas reservoir. In: Proceedings in the CPS/SPE international oil & gas conference and exhibition, China; 2010. P. 131350.
[11] Maxwell SC, Rutledge J, Jones R, Fehler M. Petroleum reservoir characterization using downhole microseismic monitoring. Geophysics 2010;75(5) (75A129–37).
[12] Das I, Zoback MD. Long-period, long-duration seismic events during hydraulic fracture stimulation of a shale gas reservoir. Lead Edge 2011;30:778–86.
[13] Sone H, Zoback MD. Mechanical properties of shale-gas reservoir rocks – part 1: static and dynamic elastic properties and anisotropy. Geophysics 2013;78: D381–D392.
[14] Sone H, Zoback MD. Mechanical properties of shale-gas reservoir rocks – part 2: ductile creep, brittle strength, and their relation to the elastic modulus. Geophysics 2013;78:D393–402.
[15] Findley WN, Lai JS, Onaran K. Creep and relaxation of nonlinear viscoelastic materials with an introduction to linear viscoelasticity. New York: Dover; 1976.
[16] Lakes RS. Viscoelastic materials. New York: Cambridge University Press; 2009.
[17] Sone H. Mechanical properties of shale gas reservoir rocks and its relation to the in-situ stress variation observed in shale gas reservoirs [PD thesis], Stanford University; 2012.
[18] Curtis JB. Fractured shale-gas systems. AAPG Bull 2002;86(11):1921–38.
[19] Zoback MD, Townend J. Implications of hydrostatic pore pressures and high crustal strength for the deformation of intraplate lithosphere. Tectonophysics 2001;336:19–30.
[20] Sleep NH, Zoback MD. Did earthquakes keep the early crust habitable? Astrobiology 2007;7:1023–32.
[21] Loucks RG, Reed RM, Ruppel SC, Jarvie DM. Morphology, genesis, and distribution of nanometer-scale pores in siliceous mudstones of the Mississippian Barnett Shale. J Sediment Res 2009;79:848–61.
[22] Ewy RT, Bovberg CA, Stankovich RJ. Shale triaxial strength alteration due to brine exposure. ARMA Paper 2008-304.
[23] Moore DE, Lockner DA. Crystallographic controls on the frictional behavior of dry and water-saturated sheet structure minerals. J Geophys Res 2004;109: B03401.
[24] Atkinson BK. Subcritical crack growth in geological materials. J Geophys Res 1984;89(B6):4077–114.
[25] Michalske TA, Freiman SF. A molecular interpretation of stress corrosion in silica. Nature 1982;295:511–2.
[26] Lockner DA. Room temperature creep in saturated granite. J Geophys Res 1993;98:475–87.
[27] Heap MJ, Baud P, Meredith PG, Bell AF, Main IG. Time-dependent brittle creep in Darley Dale sandstone. J Geophys Res 2009;114:B07203.
[28] Brantut N, Baud P, Heap MJ, Meredith PG. Micromechanics of brittle creep in rocks. J Geophys Res 2012;117:B08412.